

Unidirectionally coupled map lattice as a model for open flow systems

Oliver Rudzick* and Arkady Pikovsky

Institut für Theoretische Physik und Astrophysik, Universität Potsdam, PF 601553, D-14415 Potsdam, Germany

(Received 12 June 1996)

Spatial development of turbulence is studied with the unidirectionally coupled logistic lattice model. The transition from absolute to convective instability is described. A numerical method allowing one to compute convectively unstable states without numerical artifacts is introduced and used to construct the phase diagram. The influence of external noise on the convectively unstable regimes is investigated numerically. Different types of noise-sustained structures are described. Statistical properties of frozen periodic patterns are derived analytically and compared with the numerical results. [S1063-651X(96)10811-4]

PACS number(s): 47.27.-i, 05.45.+b

I. INTRODUCTION

Flow systems can be defined in general as systems with convective instabilities where initial perturbations are advected as they are amplified [1,2]. Examples of flow systems can be found not only in the fluid dynamics [3–5], but in a rich variety of different fields such as nonlinear optics [6], plasma physics [7], and traffic flow [8]. A characteristic feature of such systems is the way they respond to perturbations. While initial perturbations are advected outside of the system, persistent disturbances (regular or noisy) are amplified in space. As a result, one typically observes the frequency-selective amplification of noise and the formation of spatiotemporal patterns.

The usual *Ansätze* for a theoretical description of these phenomena are partial differential equations such as the Navier-Stokes [9,10] or the complex Ginzburg-Landau equation [11,5]. However, both an analytical and numerical analysis of these models is hardly feasible. Therefore it is of interest to study systems that are more convenient to treat numerically or analytically but provide, nevertheless, an understanding of the basic features of flow systems.

A class of models that have recently attracted much interest are coupled map lattices (CML's). They have been shown to exhibit a rich variety of characteristic features observed in distributed systems [12–14]. The aim of the present work is to demonstrate that some basic characteristics of flow systems can be captured qualitatively by a unidirectionally coupled map lattice. Indeed, an asymmetrical coupling leads to the advection of perturbations in one direction, similarly to flow systems. Different properties of asymetrically coupled map lattices have been discussed in Refs. [15–18]. It is interesting to mention that delay systems can also be reduced to locally unidirectionally coupled map lattices [19]. In the present paper we focus our attention on the unidirectionally coupled logistic lattice (UCLL) [20,21]. We demonstrate that sensitivity of the dynamics to the boundary perturbations makes it necessary to develop a special numerical method to simulate such a lattice; otherwise one observes many structures that are purely numerical artifacts. Having the correct numerical method, we are able to model a realis-

tic noisy environment and to investigate the arising noise-sustained structures quantitatively.

The paper is organized as follows. The UCLL model is described in Sec. II. In Sec. III we give a comprehensive analysis of the behavior of the model for the temporally constant boundary condition. In particular, we demonstrate that the truncation errors can grow in an uncontrollable way if one tries to compute convectively unstable solutions. We present a method to avoid numerical artifacts and use it to construct the phase diagram. Based on the knowledge of the behavior for the temporally constant boundary condition, we investigate in Sec. IV the response of the model to a small boundary noise. We describe different noise-sustained structures and present a statistical analysis of spatiotemporal dislocations arising in a particular region of parameters of the logistic map. In Sec. V we discuss the relation of the model under investigation to the regimes observed in the experiments with the Taylor-Couette flow.

II. THE UNIDIRECTIONALLY COUPLED MAP LATTICE

Coupled map lattices [12,13] are models with discrete time t and discrete spatial coordinate x but continuous state $u(x,t)$. The dynamics is given by a nonlinear local mapping $u \rightarrow f(u)$ and a linear coupling operator \hat{D} , which in the case of nearest-neighbor interaction couples sites $x-1$, x , and $x+1$ to produce a field at site x . In the special case of unidirectional coupling only sites $x-1$ and x influence site x and the coupling operator becomes

$$\hat{D}(u) = (1 - \epsilon)u(x,t) + \epsilon u(x-1,t),$$

where ϵ is the coupling constant. The dynamics of the lattice is given by

$$u(x,t+1) = (1 - \epsilon)f(u(x,t)) + \epsilon f(u(x-1,t)) \quad (1)$$

together with the boundary condition $u(0,t)$ and the initial condition $u(x,0)$.

We focus our investigations on the UCLL, which is given by (1) with the logistic map

$$f(u) = 1 - \alpha u^2 \quad (2)$$

*Electronic address: WWW: <http://www.agnld.uni-potsdam.de/>

as the local nonlinear transformation. The map (2) demonstrates the transition to chaos at $\alpha = \alpha_c \approx 1.41$ via period doublings. Our main aim is to describe different regimes in the lattice (1) and (2) in their dependence on the parameters ϵ , α and the boundary and initial conditions.

III. CONSTANT BOUNDARY CONDITIONS

Boundary conditions play an important role in the flow systems. We start our study with the simplest possible but, as we will see below, nontrivial boundary condition: the constant boundary field $u(0,t) = u^0 = \text{const}$.

A. Temporally constant solutions

For the constant boundary condition $u(0,t) = u^0$ the dynamics at the first site $x=1$ is given by

$$u(1,t+1) = (1-\epsilon)f(u(1,t)) + \epsilon f(u^0), \quad (3)$$

which is a parabolic map with parameters depending on ϵ , α , and u^0 . In some parameter range it has a stable fixed point $u^*(1)$ as an attractor. Thus the dynamics at the site $x=2$ is also given by a parabolic map with parameters depending on ϵ , α , and $u^*(1)$. Repeating the arguments, we can conclude that a temporally constant stable (with respect to temporal perturbations) state in the whole lattice is possible if the parabolic maps at all sites have a stable fixed point as an attractor.

The parameter region with temporally constant solutions can be determined analytically. A detailed analysis is done in the Appendix; here we only summarize the results.

Let u_{\pm}^* denote the stable and unstable fixed points of the uncoupled logistic map (2) and $u^*(x)$ is the temporally constant solution on the lattice site x . If the coupling constant ϵ satisfies

$$\epsilon > 1 - \frac{3}{4\alpha} := \epsilon_{\min}, \quad (4)$$

then for each $u^0 \in (u_{-}^*, -u_{+}^*)$ there exists only a temporally constant state as an attractor. In this case the states at the sites $x-1$ and x are related as

$$\begin{aligned} u^*(x) &= \frac{-1 + \sqrt{1 + 4(1-\epsilon)\alpha[1 - \epsilon\alpha(u^*(x-1))^2]}}{2(1-\epsilon)\alpha} \\ &=: G(u^*(x-1)) \end{aligned} \quad (5)$$

[see Eq. (A2)]. The map $u^*(x) \rightarrow G(u^*(x))$ is the spatial map introduced in [20]. For temporally constant states the spatial pattern can be obtained from an orbit of $G(u^*(x))$ with u^0 as an initial condition. With increasing ϵ the spatial map undergoes a period-doubling cascade to chaos, so that one can observe either spatially constant, spatially periodic, or spatially chaotic states for $x \rightarrow \infty$.

B. Stability properties and numerical problems

We have derived the domain of the existence of temporally constant solutions from the condition of stability of the fixed point at each lattice site. This is the temporal stability to perturbations of initial conditions, indicated by the nega-

tive usual Lyapunov exponent, which means the absence of absolute instability. This, however, does not exclude the possibility of convective instability, when an initial perturbation at site x_0 decreases at this site, but produces large perturbations for $x > x_0$. This downflow growth of perturbations is a characteristic feature of flow systems.

One of the ways to characterize the convective instability is to calculate the comoving Lyapunov exponent [22,18]; this is possible for statistically spatially homogeneous states. In the case of a spatially homogeneous solution, which can be constant in time (in this case it is represented by a fixed point of the spatial map G) or be time dependent, the comoving Lyapunov exponent depending on the reference frame velocity v can be calculated analytically [14,16]:

$$\lambda(v) = (1-v) \ln \left(\frac{1-\epsilon}{1-v} \right) + v \ln \left(\frac{\epsilon}{v} \right) + \Lambda_m, \quad (6)$$

where Λ_m is the Lyapunov exponent of the uncoupled map. From Eq. (6) we can see that λ becomes maximal in a reference frame comoving with the velocity $v = \epsilon$ and that the maximum value is given by Λ_m . The relation between $\lambda(v)$ and the usual Lyapunov exponent Λ is given by $\Lambda = \lambda(v \rightarrow 0) = \ln(1-\epsilon) + \Lambda_m$.

The type of stability depends on the parameters Λ_m, ϵ . If the orbit of the uncoupled logistic map is stable, i.e., $\Lambda_m < 0$, then $\lambda(v) < 0$ for all v and the homogeneous solution is absolutely stable. An unstable orbit of the logistic map with $\Lambda_m > 0$ produces an absolutely unstable uniform solution for small ϵ . By increasing the coupling it can be turned into a convectively unstable solution with $\lambda(0) < 0$.

An absolutely unstable homogeneous state is sensitive to initial conditions and can be realized only if they are homogeneous as well. On the other hand, in the case of convective instability initial perturbations are moved away from the boundary $x=0$, so a temporally constant (or periodic) state is, in principle, possible.

Next we want to discuss problems arising when convectively unstable solutions of the lattice are calculated numerically. If one computes the stable fixed point of a nonlinear map by iterating this map for a large number of steps, one will observe that in most of the cases the iteration does not converge precisely to the fixed point. Instead one will notice some oscillations in the last digits caused by truncation errors. These oscillations (usually they have period 2) act as an external time-periodic force on the next site, as is seen from (1). If the solution is convectively unstable, these perturbations are amplified downflow leading to transitions to some time-dependent states. This is the reason why, when computing convectively unstable solutions, one observes spatiotemporal period-doubling downflow [14,20,23].

If truncation errors are present, the orbit on a lattice site can be written as $u(x,t) = u^*(x)[1 + \delta(t)]$, where $\delta(t)$ denotes the time dependence caused by numerical effects. To get rid of the numerical artifacts, we have to suppress all changes in $u(x,t)$ smaller than the amplitude of the signal $\delta(t)$, which means a correction in the last digits. This can be done easily, e.g., by performing the calculations in double precision and converting the value of $u(x-1, t-1)$ to single precision before using it to calculate the value of $u(x,t)$. With this method we have computed the solution of the lat-

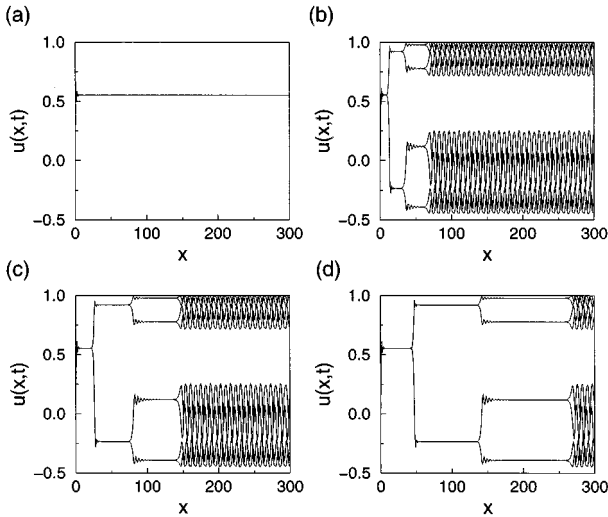


FIG. 1. Comparison between the solution of the UCLL for $\epsilon=0.5$ and $\alpha=1.45$ calculated with the method described in the text (a) and from iterations without suppressing the truncation errors using single precision (b), double precision (c), and quadruple precision (d). The spatial period doublings are the numerical artifact. The boundary condition was $u^0=0$.

tice (1) and (2) for $\alpha=1.45$, $\epsilon=0.5$, and $u_0=0$ as the boundary condition [Fig. 1(a)]. As follows from (4), for these parameter values only a temporally constant state with $u^*(x) \rightarrow u_+^*$ for $x \rightarrow \infty$ exists as a temporally stable solution. In Figs. 1(b)–1(d) this solution is compared with the results obtained from the iterations of the lattice (1) and (2) with the usual method and different numerical precision. We can see the spatiotemporal period-doubling downflow leading to a state with spatial period 4 and temporal period 8. Their onset is a pure numerical artifact and depends on the numerical precision.

C. Phase diagram

Based on the results of Sec. III A and using the numerical method discussed above, we can construct a phase diagram for the UCLL describing the asymptotic behavior for different values of the parameters α and ϵ . Figure 2 shows this diagram for the boundary condition $u^0=0$ and initial condition $u(x,0)=u_+^*$. It can be shown that for $u^0=0$ the ϵ_{\min} defined in (4) is the border of the region with temporally constant behavior in the (α, ϵ) plane. In this region the parameter range for spatially periodic and spatially chaotic behavior can be determined from the properties of the spatial map $G(u^*(x))$ (in the spatially chaotic region small windows with spatially periodic behavior exists, but are not shown). As it was discussed above, the spatially homogeneous and temporally constant solution is convectively unstable when the fixed point u^* of $f(u)$ becomes unstable. This happens for $\alpha > 3/4$ when $f(u)$ undergoes its first period doubling.

For small values of ϵ one can observe multistability. This can be understood considering the case $\epsilon \rightarrow 0$. If the parameter α is chosen such that $f(u)$ has a stable periodic orbit, in the uncoupled lattice different attractors corresponding to different phases of the periodic orbit exist, leading to spa-

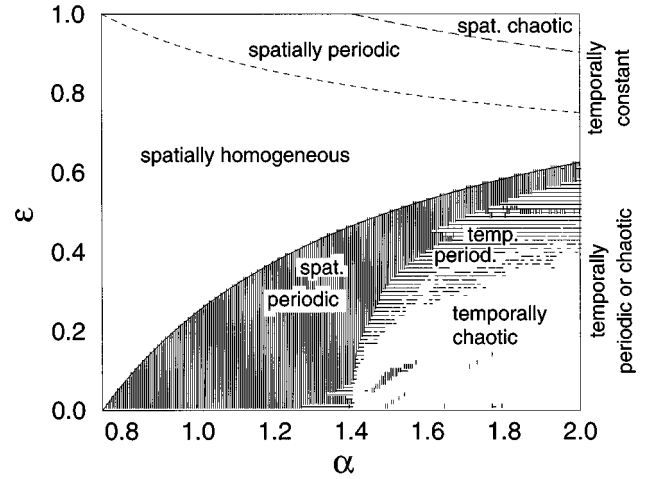


FIG. 2. Phase diagram for the UCLL with constant boundary field $u^0=0$ obtained with the method described in the text. For $\epsilon > 1 - 3/4\alpha$ and constant boundary conditions the solutions of the lattice are temporally constant.

tially homogeneous and inhomogeneous states. With increasing ϵ the spatially homogeneous state remains the solution of the lattice, while the spatially inhomogeneous states, existing for very small ϵ , disappear for large ϵ .

IV. NOISY BOUNDARY CONDITIONS

From the discussion of numerical methods above it is evident that the systems with convective instability are extremely sensitive to external perturbations. Both regular (periodic or quasiperiodic [7,24–26]) and irregular (noisy [11,27,28]) perturbations can be introduced. Below we impose noisy boundary conditions on the lattice (1) and (2).

A. Phase diagram of the noisy lattice

Here we describe the regimes observed for different values of parameters (α, ϵ) , for a particular chosen boundary condition $u(0,t)=u^* + \Delta \xi_t$ where ξ_t is a δ -correlated noise signal uniformly distributed in the interval $[-1/2, 1/2]$ and Δ measures the noise amplitude. The approximative phase diagram is shown in Fig. 3.

1. Small ϵ : Absolutely unstable states

As is discussed in Sec. III, varying α leads to the origin of new periodic or chaotic states in the lattice, while increasing ϵ turns absolutely unstable states into convectively unstable ones. In the absolutely unstable states the boundary conditions do not influence the type of dynamics far from the boundary, so this part of the phase diagram Fig. 2 remains practically unchanged. For small $\alpha \lesssim \alpha_c$ and small ϵ , spatially inhomogeneous, periodic in time patterns develop from random initial conditions. The randomness of initial conditions remains frozen (pinned) due to multistability. We denote this regime as spatially frozen random patterns (SFRPs); see Fig. 4. As the coupling increases, these patterns start to move away from the boundary $x=0$ and a spatially homogeneous time-periodic state is observed.

For large $\alpha \gtrsim \alpha_c$ the spatiotemporal chaos usual for coupled map lattices is observed (the shaded area in Fig. 3).

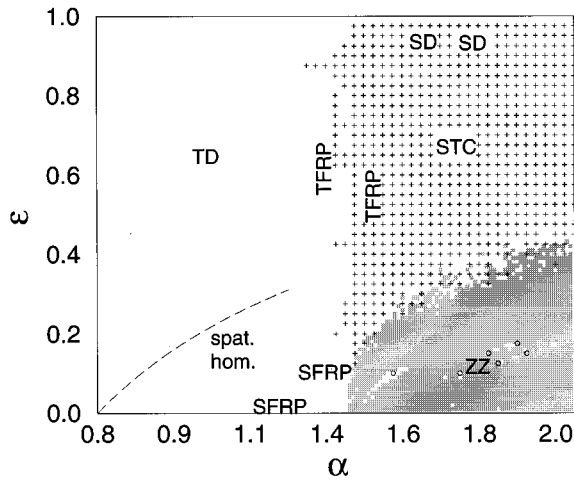


FIG. 3. Phase diagram for the noisy UCLL. The boundary condition was uniformly distributed δ -correlated noise with amplitude $\Delta = 10^{-5}$. Different regimes are described in the text.

Inside this region there are small pieces of stable behavior, such as zigzag (ZZ) patterns at $\alpha \approx 1.8$, reported in Fig. 5.

2. Large ϵ : Convectively unstable states and noise-sustained patterns

If the temporally constant state observed for a constant boundary condition is convectively unstable, even small time-dependent boundary perturbations can drastically change the dynamics, producing noise-sustained structures [11]. For small values of α these structures are relatively regular. For $0.75 < \alpha < 1.25$ the uncoupled map has an unstable fixed point and a stable period-2 orbit. If the perturbation at the boundary were a purely periodic field with period

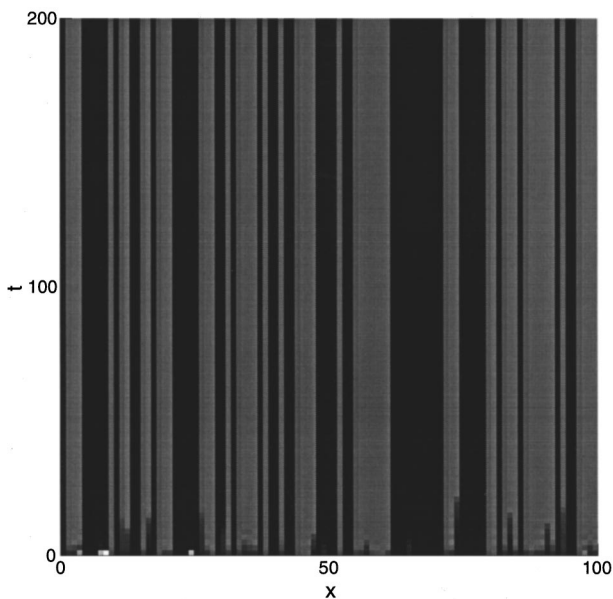


FIG. 4. Gray-scale plot of the field $u(x,t)$ with SFRPs in the x - t plane for $A = 1.2$, $\epsilon = 0.05$, and $\Delta = 10^{-5}$, plotted per two time steps. The dark areas correspond to the maxima of the field distribution.

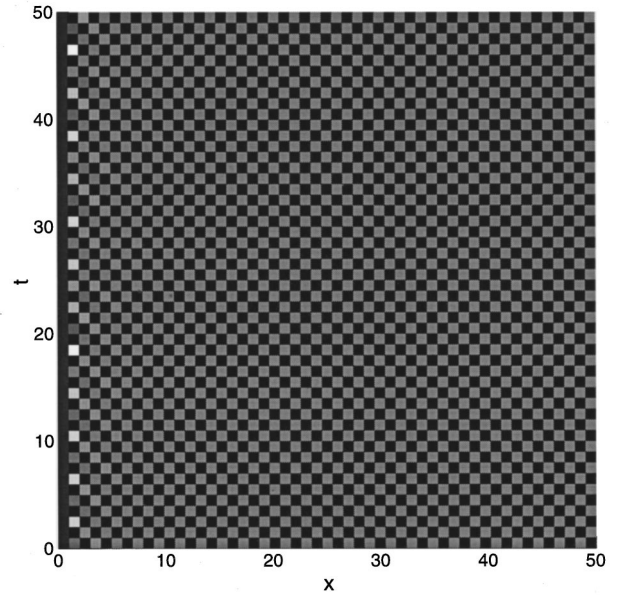


FIG. 5. Field distribution with a ZZ pattern for $A = 1.8$, $\epsilon = 0.15$, and $\Delta = 10^{-5}$. The pattern has both temporal and spatial period 2.

2, one would observe pure period-2 oscillations at each lattice site. The phase of these oscillations (which can be either 0 or π) is adjusted to the phase of the boundary field. In the case of a noisy boundary field both phases are possible and a regime of irregular switchings between phases 0 and π is observed (see Fig. 6 and the bottom panel in Fig. 10). We call this regime temporal dislocations (TDs) and describe it in more details in Sec. IV B below. It is important that, although the patterns appearing are random, they are not cha-

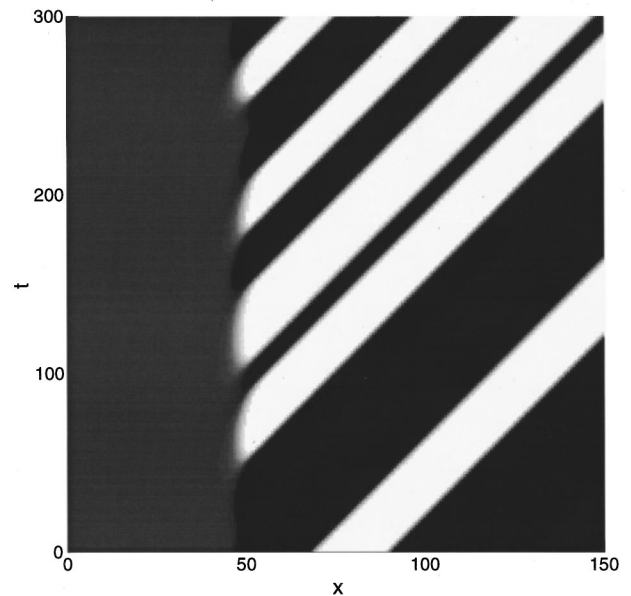


FIG. 6. Field distribution for $A = 1.0$, $\epsilon = 0.5$, and $\Delta = 10^{-12}$, plotted per two time steps. The spatial growth of fluctuations and development of patterns ends at $x \approx 50$. Black and white stripes at $x > 50$ correspond to period-2 oscillations with different phases, advected with velocity approximately equal to 0.5.

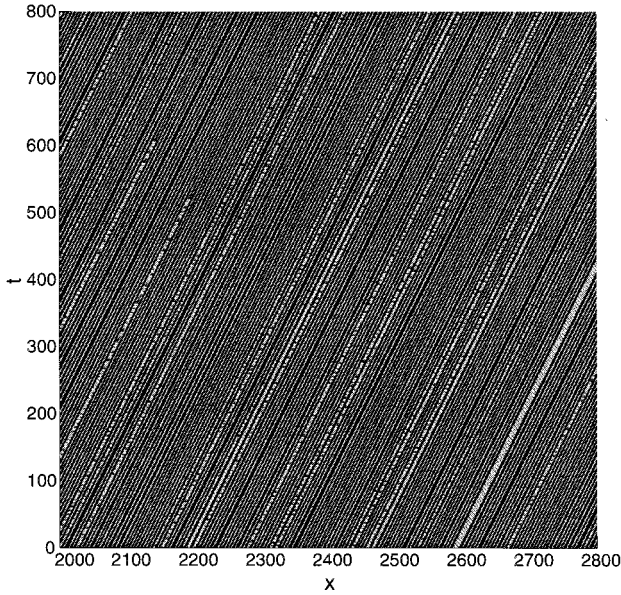


FIG. 7. Field distribution with TFRPs for $A=1.6$, $\epsilon=0.5$ and $\Delta=10^{-5}$, plotted per two time steps.

otic and remain frozen, being advected with a velocity $V \approx \epsilon$. The noise-sustained structure is stable: small noisy perturbations added to it at some large x are not amplified downflow.

As the parameter α increases and the period-doubling bifurcations take place in the uncoupled logistic map, the frozen patterns become more complicated and one cannot consider them as consisting of large coherent patches with dislocations between them. We refer to this regime as to temporally frozen random patterns (TFRPs). An example of such a pattern is reported in Fig. 7.

For $\alpha \geq \alpha_c$ the logistic map (2) demonstrates chaos. Correspondingly, the noise-sustained structures become chaotic

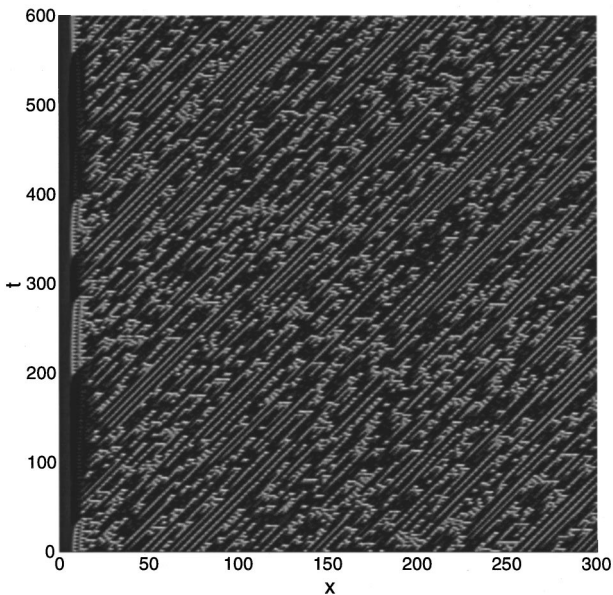


FIG. 8. Field distribution with STC for $A=1.8$, $\epsilon=0.5$, and $\Delta=10^{-5}$, plotted per two time steps.

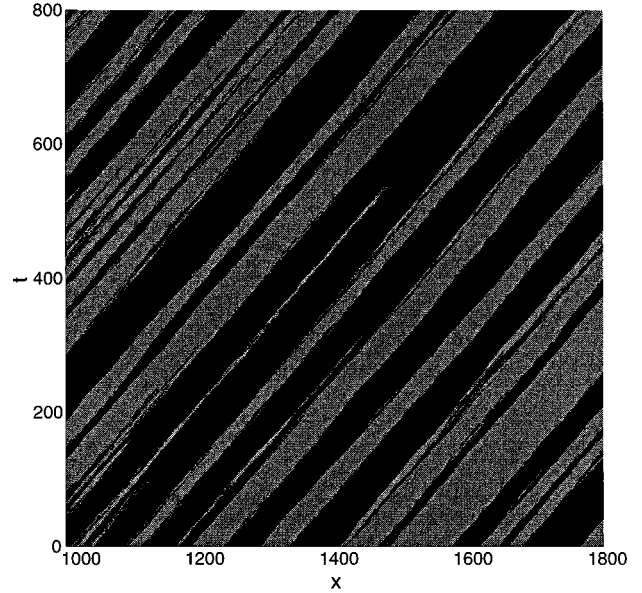


FIG. 9. Field distribution with SDs for $A=1.8$, $\epsilon=0.9$, and $\Delta=10^{-5}$, plotted per two space steps).

and a spatiotemporal chaos (STC) is observed (Fig. 8). Here small perturbations added at some large x increase downflow; the states with secondary convective instability detected in this way are marked with pluses in Fig. 3. Windows of regular behavior can be found inside chaos. One such regime is presented in Fig. 9, where frozen patches with spatial period 2 are created with dislocations between them [we call this state spatial dislocations (SDs)].

B. Statistical description of the dislocations

Here we quantify statistical properties of the regime with temporal dislocations described in Sec. IV A (regime TD in the phase diagram Fig. 3). This regime consists of frozen coherent patterns, advected with a constant velocity $V \approx \epsilon$ through the lattice. Let us consider the time series of the field on a lattice site far from the boundary $x=0$. This lattice site is passed by the spatially homogeneous domains. Therefore one observes patches of period-2 motion interrupted by phase shifts due to passages of the domain boundaries (bottom panel in Fig. 10). We call these phase shifts dislocations. We concentrate our consideration on the average interval between dislocations T_{disl} . This is a characteristic correlation time of the field, and due to the frozen state of the patterns it determines a characteristic spatial scale as well.

To find a relation between T_{disl} and the noise amplitude Δ we consider the spatial development of boundary noise leading to the formation of dislocations (Fig. 10). If the noise is small, its initial development can be described in the linear approximation. Writing the field as $u(x,t) = u^* + w(x,t)$, for the small perturbation $w(x,t)$ we get

$$w(x,t+1) = f'(u^*)[(1-\epsilon)w(x,t) + \epsilon w(x-1,t)], \quad (7)$$

with a boundary condition $w(0,t)$. This equation can be easily solved with the Fourier method. Assuming that $w(x,t) = w_x e^{i\omega t}$, we obtain from (7), for the complex amplitude w_x , the relation

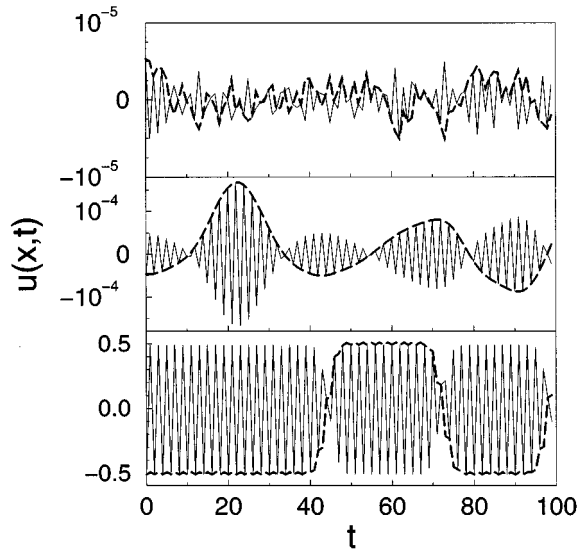


FIG. 10. Time series of the field $[u(x,t) - \langle u \rangle_t]$ (solid line) and of the amplitude $[u(x,t) - \langle u \rangle_t](-1)^t$ (dashed line) on different lattice sites for $\alpha = 1$, $\epsilon = 0.5$, and $\Delta = 10^{-5}$ in the regime TD. From top to bottom: $x = 1$, the time series is dominated by the stochastic boundary condition; $x = 10$, the time series is in the linear region, with a nearly Gaussian distribution being formed; $x = 50$, the time series with temporal dislocations is in the nonlinear region with saturated amplitude.

$$w_x e^{i\omega} = f'(u^*)[(1 - \epsilon)w_x + \epsilon w_{x-1}], \quad (8)$$

so that the perturbation field can be written as

$$w(x,t) = w_0 (\mathcal{A}(\omega))^x e^{i\omega t}, \quad (9)$$

with $\mathcal{A}(\omega)$ being a complex spatial growth factor

$$\mathcal{A}(\omega) = \frac{\epsilon f'(u^*)}{e^{i\omega} - (1 - \epsilon)f'(u^*)}. \quad (10)$$

Using the Fourier representation of the noisy boundary field, we obtain from (9) the transformation of the power spectrum $S(x, \omega)$ as

$$S(x, \omega) = S(0, \omega) |\mathcal{A}(\omega)|^{2x}. \quad (11)$$

If the noise at the boundary is δ correlated we have $S(0, \omega) \equiv \text{const}$ and therefore $S(x, \omega) \sim |\mathcal{A}(\omega)|^{2x}$, which gives, together with (10),

$$S(x, \omega) \sim \left(\frac{a}{b \cos \omega + c} \right)^x, \quad (12)$$

where

$$a := [\epsilon f'(u^*)]^2, \quad b := -2(1 - \epsilon)f'(u^*), \quad c := \frac{b^2}{4} + 1. \quad (13)$$

Because $b > 0$, the amplification factor $|\mathcal{A}(\omega)|$ has a maximum at $\omega = \pi$. This maximum in the spectrum (12) becomes

very sharp for large x , which means that the oscillations with period 2 dominate the process (Fig. 10). It is convenient to represent such a signal as

$$w(x,t) = A(x,t)(-1)^t, \quad (14)$$

where A is an amplitude. If the process $w(x,t)$ is Gaussian (even if the boundary noise has another distribution, in the course of filtering a Gaussian signal appears), the amplitude A has a Gaussian distribution as well, and therefore changes sign. These sign changes can be interpreted as dislocations because they correspond to the shifts of the phase of the period-2 oscillations by π . Thus the statistics of dislocations is described by the statistics of zero crossings of $A(x,t)$.

For a Gaussian process with zero mean value the average number of zero crossings in a time interval $(0, T)$ can be expressed through the power spectrum as [29]

$$\mathcal{E}\{C_u(0, T)\} = \frac{T}{\pi} \left(\frac{\lambda_2}{\lambda_0} \right)^{1/2}, \quad (15)$$

where λ_{2k} denotes the $2k$ th spectral moment of the signal

$$\lambda_{2k} = \int_0^\infty \omega^{2k} S(\omega) d\omega.$$

The averaged interval between dislocations $T_{\text{disl}}(x)$ is therefore

$$T_{\text{disl}}(x) = T / \mathcal{E}\{C_u(0, 1)\} = \pi \left(\frac{\lambda_0(\tilde{S})}{\lambda_2(\tilde{S})} \right)^{1/2}, \quad (16)$$

where $\tilde{S}(x, \omega) = S(x, \omega + \pi)$ is the power spectrum of the process $A(x, t)$.

For large x , calculation of the spectral moments

$$\lambda_{2k} = \int_\pi^{2\pi} (\omega - \pi)^{2k} \left(\frac{a}{b \cos \omega + c} \right)^x d\omega \quad (17)$$

can be performed with the help of the Laplace method, giving, to leading order,

$$\frac{\lambda_0}{\lambda_2} = \frac{bx}{c - b}. \quad (18)$$

Thus the average interval between dislocations

$$T_{\text{disl}}(x) = \pi \sqrt{\frac{bx}{c - b}}. \quad (19)$$

increases downflow as a square root of the distance from the boundary.

The relation (19) is derived in the linear approximation. The nonlinearity leads to saturation of the amplitude A and the dislocations become frozen, so that T_{disl} saturates as well. Therefore, to describe statistical properties in the nonlinear regime, we can use the relation (19) with x replaced by the characteristic length of linear region L_{lin} . Because in the linear region the field grows in space exponentially, we can estimate the dependence of its length on the amplitude of the boundary noise as $L_{\text{lin}} \sim -\ln(\Delta)$, which gives

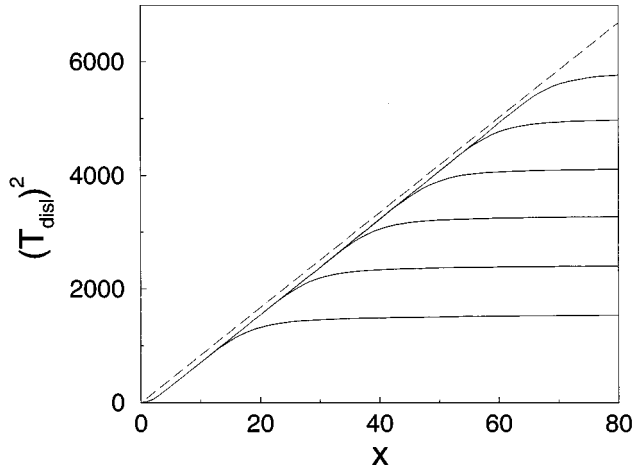


FIG. 11. Average interval between dislocations vs distance from the boundary for $\alpha=1$, $\epsilon=0.5$, and different noise amplitudes (solid lines). From bottom to top: $\Delta=10^{-2}$, $\Delta=10^{-4}$, $\Delta=10^{-6}$, $\Delta=10^{-8}$, $\Delta=10^{-10}$, and $\Delta=10^{-12}$. The dashed line shows the prediction of Eq. (19).

$$T_{\text{disl}} \sim [-\ln(\Delta)]^{1/2}. \quad (20)$$

To check the validity of the theoretical predictions made above we have studied the spatial development of the averaged dislocation interval (Fig. 11). In the linear range Eq. (19) is valid and for large x the saturation is observed. The stationary values of T_{disl} in the nonlinear region (Fig. 12) agree rather well with the theoretical prediction (20).

V. CONCLUSION

We have studied the unidirectionally coupled logistic lattice model. For constant boundary condition and small coupling, nonstationary periodic and chaotic regimes are observed. If the coupling is strong, a temporally constant state

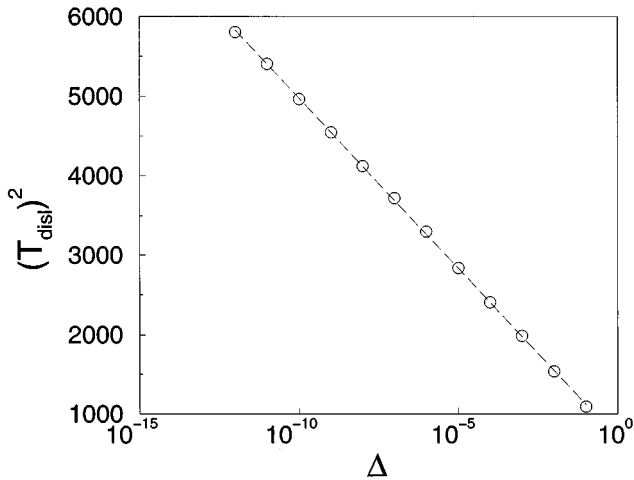


FIG. 12. Average interval between dislocations vs noise amplitude Δ for $\alpha=1.0$ and $\epsilon=0.5$. The linear dependence (dashed line) agrees with (20).

(which can be spatially homogeneous, periodic, or chaotic) is the only attractor. This state can be convectively unstable, and we have pointed out that this leads to the risk of numerical artifacts due to the possible growth of truncation errors. A simple numerical method allowing one to avoid these artifacts has been introduced and used for the construction of the phase diagram.

Convectively unstable states are sensitive to perturbations, and in order to model real physical situations, one has to include noise. Taking noisy boundary conditions, we have found a rich variety of spatiotemporal patterns in the lattice. For small nonlinearity, when the logistic map has periodic attractors, patches of frozen periodic patterns with dislocations between them are moving through the lattice. The averaged size of the patches is related to the noise amplitude with the relation (20). For large nonlinearity, noise-sustained chaotic structures are observed.

We now discuss the relation of the model to the experimental studies of flow systems. Recently, experiments have been performed on the formation of vortices in the Taylor-Couette system with imposed axial throughflow [5,30]. It consists of fluid contained between two concentric cylinders with the inner one rotating and with throughflow imposed in the direction of the cylinder's axis. For a significant range of control parameters, rotating the inner cylinder causes the structureless base flow to become convectively unstable and leads to the existence of a stable secondary flow (Taylor vortices). In the experiments the velocity of the throughflow determines the transition from absolute to convective instability and therefore corresponds to the coupling ϵ . On the other hand, rotation velocity of the cylinders determines nonlinearity of the vortices and corresponds to the parameter of the logistic map α . Our observation of the spatial development of time-periodic structures from the boundary noise is similar to the spatial development of traveling Taylor vortices in the flow under conditions of convective instability [see Fig. 7(a) in [5]].

The similarities between the Taylor-Couette flow and the UCLL model are significant, although the nature of the perturbations in both systems is different. In the Taylor-Couette flow the source of perturbations is thermal noise, which is present in the whole system, while in the CML we have applied the noise only at the boundary. Simulations of the UCLL with additive noise acting on each lattice site have shown no qualitative difference compared to the case of purely boundary noise. This is not surprising because due to spatial growth of perturbations the boundary noise dominates.

However, the discreteness of space and time in the UCLL leads to essential restrictions in the applicability of the coupled map models to continuous flows. The most important is discreteness in time: while in the Taylor-Couette flow the temporal spectrum becomes more and more narrow downflow, in the map model the phase dislocations are frozen and no further evolution in the nonlinear regime is observed. For the realistic models of the Taylor-Couette flow with continuous time we refer to Refs. [5,10].

Although there are important restrictions due to the discreteness in space and time, we have demonstrated that it is in principle possible to mimic basic features of complicated flow systems with simple models such as UCLLs. In this

context it would be interesting to study modifications of these models aimed at obtaining a more realistic description of experimental systems. For example, replacing the unidirectional coupling with an asymmetric one may be important for the investigation of the regimes at the boundary between convective and absolute instability. Another interesting question is how far the results for the map models can be extended to more complicated systems such as chains of oscillators or partial differential equations.

ACKNOWLEDGMENTS

We thank W. Jansen, K. Kaneko, B. Kerner, J. Kurths, S. Lepri, A. Politi, A. Torcini, and H. Voss for useful discussions. The work of O.R. has been supported by a grant (Promotionsstipendium) from the state of Brandenburg.

APPENDIX: EXISTENCE OF TEMPORALLY CONSTANT SOLUTIONS

Let $u(x-1, t) \equiv u^*(x-1)$ be a temporally constant solution of the lattice (1) and (2) on the $(x-1)$ th lattice site. Then the dynamics of the x th lattice site is given by

$$u(x, t+1) = \beta - \gamma(u(x, t))^2, \quad (\text{A1})$$

with $\beta = 1 - \epsilon\alpha(u^*(x-1))^2$ and $\gamma = \alpha(1 - \epsilon)$. This is also a form of the logistic map that can be renormalized to the form (2) with $\alpha' = \beta\gamma$. For $\beta\gamma > -1/4$ this map has two fixed points $u_+^*(x), u_-^*(x)$ given by

$$u_{\pm}^*(x) = \frac{-1 \pm \sqrt{1 + 4(1 - \epsilon)\alpha[1 - \epsilon\alpha(u^*(x-1))^2]}}{2(1 - \epsilon)\alpha}. \quad (\text{A2})$$

The upper fixed point $u_+^*(x)$ is stable for $-1/4 < \beta\gamma < 3/4$ and the lower fixed point $u_-^*(x)$ is always unstable. Rewriting the stability condition $\beta\gamma < 3/4$ as

$$[u_+^*(x)]^2 > \frac{1}{\epsilon\alpha} \left(1 - \frac{3}{4\alpha(1 - \epsilon)} \right), \quad (\text{A3})$$

we can see that for

$$\epsilon > 1 - \frac{3}{4\alpha} := \epsilon_{\min}, \quad (\text{A4})$$

when the right-hand side of (A3) is negative, on the whole lattice the root $u_+^*(x)$ must be stable as far as it exists. In this case (A2) reduces to (5) and defines the ‘‘spatial map’’ $u_+^*(x+1) = G(u_+^*(x))$ introduced in [20].

The fixed points of the uncoupled logistic map u_-, u_+ are also the fixed points of the spatial map G ; they correspond to temporally constant and spatially homogeneous states of the lattice. It can be shown that for $\epsilon < 1$ the interval $[u_-, -u_-]$ is an invariant set of the spatial map and outside of this interval (5) is not defined. Therefore, if $\epsilon > \epsilon_{\min}$ and $u^0 \in (u_-, -u_-)$, the temporally constant solution establishes in the whole lattice. The spatial pattern is represented by an orbit of the spatial map with u^0 as the initial condition. The map G undergoes with increasing ϵ a period-doubling cascade to chaos. In the chaotic regime of G a spatially chaotic temporally constant state is observed: it is linearly stable to small perturbations of initial conditions on the lattice sites, but sensitive to temporally constant perturbations of boundary condition.

For $\epsilon < \epsilon_{\min}$ the right-hand side of (A3) is positive. Thus the condition (A3) may be violated at some x . At this site the map (A1) has no stable fixed points and a stable time-dependent (periodic or chaotic) regime appears. The transition to time-dependent state always happens for

$$\epsilon \leq 1 - \frac{1}{\sqrt{1 + 4\alpha - 1}} =: \epsilon_{\min_2}, \quad (\text{A5})$$

when the right-hand side of (A3) exceeds the value of $(u_-^*)^2$. Thus $\epsilon > \epsilon_{\min_2}$ is a necessary condition for the existence of linearly stable, temporally constant solutions in the lattice (1) and (2).

-
- [1] E.M. Lifshitz and L.P. Pitaevskii, *Physical Kinetics* (Pergamon, Oxford, 1981).
 - [2] M.C. Cross and P.C. Hohenberg, *Rev. Mod. Phys.* **65**, 851 (1993).
 - [3] P. Huerre and P.A. Monkewitz, *Annu. Rev. Fluid Mech.* **22**, 473 (1990).
 - [4] M.F. Schatz *et al.*, *Phys. Rev. Lett.* **66**, 1579 (1991).
 - [5] K.L. Babcock, G. Ahlers, and D.S. Cannell, *Phys. Rev. E* **50**, 3670 (1994).
 - [6] K. Otsuka and K. Ikeda, *Phys. Rev. A* **39**, 5209 (1989).
 - [7] N.S. Ginzburg, A.S. Pikovsky, and A.S. Sergeev, *Sov. J. Commun. Technol. Electron.* **34**, 38 (1989).
 - [8] B. Kerner (private communication).
 - [9] P. Huerre and P.A. Monkewitz, *J. Fluid Mech.* **159**, 151 (1985).
 - [10] H.W. Müller, M. Lücke, and M. Kamps, *Phys. Rev. A* **45**, 3714 (1992).
 - [11] R.J. Deissler, *J. Stat. Phys.* **40**, 371 (1985).
 - [12] *Theory and Applications of Coupled Map Lattices*, edited by K. Kaneko (Wiley, Chichester, 1993).
 - [13] *CHAOS* **2** (3) (1992) special issue on coupled map lattices edited by K.Kaneko.
 - [14] J.P. Crutchfield and K. Kaneko, in *Directions in Chaos*, edited by B.-L.Hao (World Scientific, Singapore, 1987), Vol. 1.
 - [15] K. Kaneko, *Phys. Lett. A* **111**, 321 (1985).
 - [16] T. Bohr and D. A. Rand, *Physica D* **52**, 532 (1991).
 - [17] I. Aranson, D. Golomb, and H. Sompolinsky, *Phys. Rev. Lett.* **68**, 3495 (1992).
 - [18] A.S. Pikovsky, *CHAOS* **3**, 225 (1993).
 - [19] S. Lepri, *Phys. Lett. A* **191**, 291 (1994).
 - [20] F.H. Willeboordse and K. Kaneko, *Phys. Rev. Lett.* **73**, 533 (1994).
 - [21] F.H. Willeboordse and K. Kaneko, *Physica D* **86**, 428 (1995).
 - [22] R.S. Deissler and K. Kaneko, *Phys. Lett. A* **119**, 397 (1987).

- [23] A.S. Pikovsky, Phys. Lett. A **156**, 223 (1991).
- [24] A.S. Pikovsky, Phys. Lett. A **137**, 121 (1989).
- [25] A.S. Pikovsky, Sov. J. Commun. Technol. Electron. **34**, 1989 (1989).
- [26] A.S. Pikovsky, Sov. J. Commun. Technol. Electron. **7**, 61 (1988).
- [27] R. Deissler, Physica D **25**, 233 (1987).
- [28] R.J. Deissler, Physica D **18**, 467 (1986).
- [29] H. Cramér and M.R. Leadbetter, *Stationary and Related Stochastic Processes* (Wiley, New York, 1967).
- [30] A. Tsameret and V. Steinberg, Phys. Rev. Lett. **67**, 3392 (1991).